Density-dependent hopping for ultracold atoms immersed in a Bose-Einstein-condensate vortex lattice

R. H. Chaviguri,[1] T. Comparin,[2] M. Di Liberto,[2,3] and M. A. Caracanhas[1]

[1]*Instituto de Física de São Carlos, Universidade de São Paulo, CP 369, São Carlos, SP, 13560-970, Brazil*

[2]*INO-CNR BEC Center and Dipartimento di Fisica, Università di Trento, 38123 Povo, Italy*

[3]*Center for Nonlinear Phenomena and Complex Systems, Université Libre de Bruxelles, CP 231, Campus Plaine, B-1050 Brussels, Belgium*

(Received 1 December 2017; published 8 February 2018)

Both mixtures of atomic Bose-Einstein condensates and systems with atoms trapped in optical lattices have been intensely explored theoretically, mainly due to the exceptional developments on the experimental side. We investigate the properties of ultracold atomic impurities (bosons) immersed in a vortex lattice of a second Bose-condensed species. In contrast to the static optical-lattice configuration, the vortex lattice presents intrinsic dynamics given by its Tkachenko modes. These excitations induce additional correlations between the impurities, which consist of a long-range attractive potential and a density-dependent hopping, described here in the framework of an extended Bose-Hubbard model. We compute the quantum phase diagram of the impurity species through a Gutzwiller ansatz and through the mean-field approach, and separately identify the effects of the two additional terms, i.e., the shift and the deformation of the Mott-insulator lobes. The long-range attraction, in particular, induces the existence of a triple point in the phase diagram, in agreement with previous quantum Monte Carlo calculations [Chaviguri *et al.*, Phys. Rev. A **95**, 053639 (2017)].

DOI: 10.1103/PhysRevA.97.023614

I. INTRODUCTION

Ultracold atoms in optical lattices provide access to a rich set of interesting quantum-physics systems. This is especially due to the high experimental control achievable and to the possibility of reaching strongly correlated phases [1–3]. Both bosonic and fermionic atomic species can be trapped in optical lattices, with several allowed geometries and the possibility of engineering different kinds of interactions. The paradigmatic example is the case of spinless bosons with short-range interactions, described via the ordinary Bose-Hubbard (BH) model [4–6]. Within this model, hopping between sites favors a delocalized phase, while the on-site interatomic repulsion suppresses density fluctuations and favors localization. Such competition results in a quantum phase transition between the Mott-insulator (MI) and superfluid (SF) phases, and its signature was clearly identified in a breakthrough experiment [7]. Among the several possible extensions beyond this example, we focus on the addition of long-range interactions and of density-dependent hopping.

In the original BH model, only interactions between atoms on the same site are considered, as the interatomic potential is already negligible at the distance of one lattice constant. For longer-ranged interactions, however, one also has to include atomic pairs at larger distance, starting with those on neighboring sites. This is the case for atomic species with large dipolar moment, for which the long-ranged dipole-dipole interaction is present. The corresponding extended Bose-Hubbard model (EBH) was recently realized in experiments with a gas of erbium atoms in a three-dimensional lattice [8]. On the theoretical side, there exist several predictions for systems with long-range interactions. In one dimension, they include the peculiar Haldane-insulator phase [9], while in higher dimensions they range from density waves to supersolidity, for both hard-core and soft bosons; see reviews in Refs. [10,11].

A different extension of the BH model consists of adding terms where the hopping between two sites also depends on the two corresponding densities. In the study of the Fermi-Hubbard model, this density-dependent hopping was introduced to study ferromagnetism and superconductivity in solid-state materials [12–14]. For ultracold atoms in optical lattices, it is a term that is often negligible but in principle always present, as it is related to off-site matrix elements of the interaction term. In some cases, including the case of strong dipolar interactions, this term is non-negligible, as predicted by theory [15,16] and observed experimentally [8,17]. Alternatively, one can artificially enhance the density-dependent hopping term via Floquet driving schemes. One possibility is given by a time-dependent modulation of the s-wave scattering length [18,19], later experimentally realized [20]. Another possibility is given by near-resonant lattice shaking [21].

In this and previous works [22,23], the trapping mechanism provided by an optical lattice is replaced by the underlying vortex lattice generated in a Bose-Einstein condensate (BEC). The experimental production of vortices in ultracold dilute gases varies from a few units [24,25] to large arrays [26], arranged in the Abrikosov triangular configuration. The peculiar dynamics of the vortex lattice is characterized by the Tkachenko vibrational modes [27], which were also identified in ultracold-atom experiments [28]. Such a lattice can trap atomic impurities (that is, atoms of a different species), which are then described through a discrete lattice model.

Taking into account the dynamics of the vortex lattice, in this work we extend the effective model for the atomic impurities of Ref. [23]. The derivation of this extended Bose-Hubbard Hamiltonian (EBH) is based on the polaron transformation,

with parameters chosen through a variational approach, and the resulting model includes both the nontrivial ingredients mentioned above: a long-range interaction and a density-dependent hopping.

To explore the new features of this system we determine its phase diagram through approximate methods (based on the Gutzwiller ansatz or on a mean-field decoupling), and identify the effects of the two additional terms in the Hamiltonian. The long-range attraction is known to induce a change in the position and size of the MI regions in the phase diagram. By extending the analysis of Ref. [23], we observe that it also introduces a discontinuous transition between Mott insulators with different filling, ending at a triple point where it merges with the conventional MI/SF phase boundary. The density-dependent hopping has a positive coefficient so that its main effect is to enhance superfluidity. At a difference with the nearest-neighbor attractive interaction, this effect results in a shift of the critical hopping parameter for the MI/SF transition.

The paper is structured as follows: Sec. II corresponds to the derivation of an effective model for atomic impurities immersed in a vortex lattice BEC, while the resulting EBH model is characterized in Sec. III, followed by the conclusions in Sec. IV.

II. PHYSICAL MODEL

We consider a quasi-2D system composed of two ultracold atomic species, the majority species A and the impurity species B. The Hamiltonian of the system is the sum of three terms [23],

$$
\begin{aligned}
H_A &= \int d^2r \left[\hat{\psi}_A^\dagger(\mathbf{r}) \frac{[-i\hbar\nabla - \mathbf{A}(\mathbf{r})]^2}{2m_A} \hat{\psi}_A(\mathbf{r}) \right. \\
&\quad \left. + \hat{\psi}_A^\dagger(\mathbf{r}) V_{\text{ext}}(\mathbf{r}) \hat{\psi}_A(\mathbf{r}) + \frac{g_A}{2} (\hat{\psi}_A^\dagger(\mathbf{r}) \hat{\psi}_A(\mathbf{r}))^2 \right], \\
H_B &= \int d^2r \left[\hat{\psi}_B^\dagger(\mathbf{r}) \frac{(-i\hbar\nabla)^2}{2m_B} \hat{\psi}_B(\mathbf{r}) \right. \\
&\quad \left. + \hat{\psi}_B^\dagger(\mathbf{r}) V_{\text{ext}}(\mathbf{r}) \hat{\psi}_B(\mathbf{r}) + \frac{g_B}{2} (\hat{\psi}_B^\dagger(\mathbf{r}) \hat{\psi}_B(\mathbf{r}))^2 \right], \\
H_{AB} &= g_{AB} \int d^2r \, \hat{\psi}_A^\dagger(\mathbf{r}) \hat{\psi}_B^\dagger(\mathbf{r}) \hat{\psi}_A(\mathbf{r}) \hat{\psi}_B(\mathbf{r}),
\end{aligned} \tag{1}
$$

where $\hat{\psi}_i^\dagger(\mathbf{r})$ [$\hat{\psi}_i(\mathbf{r})$] is the creation (annihilation) operator, and m_A and m_B are the atomic masses of the two species. The two-dimensional intra- and interspecies contact interactions, $g_i = 2\sqrt{2\pi}\hbar^2 a_i/m_i l_z^i$ and $g_{AB} = \sqrt{2\pi}\hbar^2 a_{AB}/m_{AB} l_z^{AB}$, depend on the corresponding scattering lengths a_i and a_{AB} (for $i \in \{A,B\}$), and the reduced mass reads $m_{AB} = m_A m_B/(m_A + m_B)$. The transverse harmonic confinement defines the characteristic lengths $l_z^i = \sqrt{\hbar/(m_i\omega_z)}$ and $l_z^{AB} = \sqrt{\hbar/(2m_{AB}\omega_z)}$.

In addition, a synthetic magnetic field is introduced for A atoms. Within the scheme described in Ref. [29], laser beams are used to couple internal atomic states, and a magnetic-field gradient provides the inhomogeneity required to generate a nontrivial synthetic field. In the Hamiltonian, this field is represented by the pseudovector potential $\mathbf{A}$, which can be written as $\mathbf{A} = m_A\Omega \times \mathbf{r}$ (with Ω pointing in the direction orthogonal to the plane). The technique in Ref. [29] would also modify the confining potential V_{ext}, but we neglect this effect here. Up to a dozen vortices were generated in the original experiment based on this technique [30], and a method to increase this number was recently proposed [31]. Moreover, numerical solutions of the Gross-Pitaevskii equation for this system show that an extended vortex lattice can form [29,32].

The Gross-Pitaevskii equation can describe a two-dimensional vortex lattice at $T = 0$ in the quantum Hall (QH) regime [33–35]. In this regime, the occupied states are the quasidegenerate lowest Landau level $\varphi_A \propto \prod_k (z - \zeta_k)$, where $\zeta_k = (x_k + iy_k)/l$ is a complex number which represents the position of the kth vortex in the lattice [with $(x,y) = \mathbf{r}$], here normalized by the magnetic length $l = \sqrt{\hbar/m_A\Omega}$. The wave function of species A is given by $\psi_A(\mathbf{r}) = \sqrt{n_A}\varphi_A(\mathbf{r})$, where $n_A = N_A/S$ is the average atomic density and S is the total surface of the lattice.

In the QH regime, the vortex lattice is established with the population of species A much higher than the number of vortices. We require the number of B impurities to be of the same order as the number of vortices N_V, $N_B \sim N_V \ll N_A$, such that the vortex-lattice structure is not affected by their presence.

In the grand-canonical formalism, we decompose the field operator of species A into a condensed part and its fluctuations, namely $\hat{\psi}_A = \psi_A + \delta\hat{\psi}_A$. Substituting in the total Hamiltonian of Eq. (1), and keeping terms up to quadratic order in the fluctuations, yields

$$
K = \underbrace{H_B + H_{AB}^{(0)} - \mu_B \hat{N}_B}_{K_B} + \underbrace{H_{AB}^{(1)}}_{H_{\text{int}}} + \underbrace{H_A^{(0)} + H_A^{(2)}}_{K_A} \tag{2}
$$

where $\hat{N}_B$ is the impurity number operator. The upper index in the Hamiltonians of Eq. (2) indicates the expansion order in terms of the species A field fluctuation $\delta\hat{\psi}_A$. As a reminder, the validity of the Gross-Pitaevskii equation implies $H_A^{(1)} = 0$.

In the following sections, we consider the two cases where the vortex-lattice fluctuations are neglected or included, namely the static and dynamical lattice.

A. Static lattice

Disregarding the vortex lattice fluctuations, i.e., assuming the mean-field (MF) regime $\hat{\psi}_A \approx \psi_A$, the contribution of species A Hamiltonian is reduced to a constant energy shift $H_A^{(0)}$. Interspecies interactions contribute with an effective MF potential given by $H_{AB}^{(0)} = \int d^2r \, V_A(\mathbf{r}) \hat{\psi}_B^\dagger(\mathbf{r}) \hat{\psi}_B(\mathbf{r})$, where $V_A(\mathbf{r}) = n_A g_{AB} |\varphi_A(\mathbf{r})|^2$. From the result above, we note that the species A behaves like a "static" lattice for the impurity species B.

Here we consider the tight-binding regime for the impurities trapped in the vortex lattice sites, with the lattice potential amplitude $V_0 = n_A g_{AB}$ being much larger than the recoil energy $E_R = \hbar^2/(2m_B\xi_A^2)$ [36], where $\xi_A = \hbar/\sqrt{2m_A n_A g_A}$ is the healing length of species A. In the quantum Hall regime, the intervortex distance $d = 2l$ is approximately equal to $2\xi_A$ [37]. In general $d^2 = 16\Gamma_L\xi_A^2$, with $\Gamma_L = n_A g_A/2\hbar\Omega$ ($\leqslant 1$) [38] being a parameter associated with the lowest-Landau-level constraint, which is related to the vortex areal density by $N_V \sim 1/\pi d^2$.

In the tight-binding regime ($V_0 \gg E_R$), the large gap between the first and second Bloch bands allows us to only consider the lowest band to describe the behavior of the impurities. The Bloch wave function $\Phi_{\mathbf{k}}(\mathbf{r})$ for the impurities in the lattice can be related to the Wannier function $\omega_B(\mathbf{r}_i)$, which is strongly localized on the vortex sites $\mathbf{R}_i$, as $\omega_B(\mathbf{r}_i) = (1/\sqrt{N_V})\sum_{\mathbf{k}} \Phi_{\mathbf{k}}(\mathbf{r})e^{i\mathbf{k}\cdot\mathbf{R}_i}$, where $\mathbf{r}_i \equiv \mathbf{r} - \mathbf{R}_i$ and $\int d^2r|\omega_B(\mathbf{r}_i)|^2 = 1$. The field operator can be expanded in the Wannier basis as

$$\hat{\psi}_B(\mathbf{r}) = \sum_i \omega_B(\mathbf{r}_i)\,\hat{b}_i, \tag{3}$$

where $\hat{b}_i$ ($\hat{b}_i^\dagger$) destroys (creates) impurity atoms on site i. After inserting Eq. (3) in K_B, and considering only on-site interactions and nearest-neighbor hopping terms, one obtains the Bose-Hubbard Hamiltonian [5]

$$K_B^{\mathrm{BH}} = -J\sum_{\langle i,j\rangle}\hat{b}_i^\dagger\hat{b}_j + \frac{U}{2}\sum_i \hat{n}_i(\hat{n}_i - 1) - \mu_B\sum_i \hat{n}_i, \tag{4}$$

where $\hat{b}_i^\dagger\hat{b}_i = \hat{n}_i$ is the local-density operator and the first sum runs over all nearest-neighbor pairs (i,j). The hopping amplitude J and the on-site interaction energy U read

$$J = -\int d^2r\,\omega_B^*(\mathbf{r}_i)\left[-\frac{\hbar^2\nabla^2}{2m_B} + g_{AB}n_A|\varphi_A(\mathbf{r})|^2\right]\omega_B(\mathbf{r}_j), \tag{5}$$

$$U = g_B\int d^2r\,|\omega_B(\mathbf{r})|^4. \tag{6}$$

B. Dynamical lattice

The vortex lattice presents normal vibrational modes, the Tkachenko modes, which can be included in our previous model as quantum fluctuations, i.e., using a beyond MF approach for species A, with $\delta\hat{\psi}_A \neq 0$. The presence of fluctuations radically modifies the dynamics of impurities. In addition to changing the structure of the hopping and on-site energy, their inclusion generates new off-site terms in the BH Hamiltonian that significantly affect the quantum phase diagram, as described in Sec. III.

We apply the Bogoliubov canonical transformation to the fluctuation field

$$\delta\hat{\psi}_A(\mathbf{r}) = \frac{1}{\sqrt{S}}\sum_{\mathbf{q}}[u_{\mathbf{q}}(\mathbf{r})\hat{a}_{\mathbf{q}} - v_{\mathbf{q}}(\mathbf{r})\hat{a}_{\mathbf{q}}^\dagger], \tag{7}$$

with $u_{\mathbf{q}}$ and $v_{\mathbf{q}}$ being specific functions associated with the vortex lattice and $\hat{a}_{\mathbf{q}}^\dagger$ ($\hat{a}_{\mathbf{q}}$) the creation (destruction) operators of a Tkachenko mode with momentum $\mathbf{q}$ and energy dispersion $\epsilon_{\mathbf{q}}$ [34]. Using the Wannier-function expansion of Eq. (3) together with the Bogoliubov transformation in the respective Hamiltonians of Eq. (2), we obtain

$$K_B^{\mathrm{EBH}} = \sum_{\mathbf{q}}\epsilon_{\mathbf{q}}\hat{a}_{\mathbf{q}}^\dagger\hat{a}_{\mathbf{q}} - J\sum_{\langle i,j\rangle}\hat{b}_i^\dagger\hat{b}_j + \frac{U}{2}\sum_i\hat{n}_i(\hat{n}_i-1) - \mu_B\sum_i\hat{n}_i + g_{AB}\sqrt{\frac{n_A}{S}}\sum_{\mathbf{q},ij}[\Omega_{\mathbf{q}}^{ij}\hat{a}_{\mathbf{q}} + \bar{\Omega}_{\mathbf{q}}^{ij}\hat{a}_{\mathbf{q}}^\dagger]\hat{b}_i^\dagger\hat{b}_j, \tag{8}$$

where

$$\Omega_{\mathbf{q}}^{ij} = \int d^2r[\varphi_A^*(\mathbf{r})u_{\mathbf{q}}(\mathbf{r}) - \varphi_A(\mathbf{r})v_{\mathbf{q}}^*(\mathbf{r})]\omega_B^*(\mathbf{r}_i)\omega_B(\mathbf{r}_j),$$
$$\bar{\Omega}_{\mathbf{q}}^{ij} = \int d^2r[\varphi_A(\mathbf{r})u_{\mathbf{q}}^*(\mathbf{r}) - \varphi_A^*(\mathbf{r})v_{\mathbf{q}}(\mathbf{r})]\omega_B^*(\mathbf{r}_i)\omega_B(\mathbf{r}_j). \tag{9}$$

To cancel the last term in Eq. (8), we apply a unitary transformation [39] that renormalizes the coefficients of the total Hamiltonian to account for the vibrational modes. This gives a polaronic extended Bose-Hubbard Hamiltonian for the impurity atoms [40,41]. We consider $\tilde{K}_B = e^{-\mathcal{U}}K_B^{\mathrm{EBH}}e^{\mathcal{U}} = K_B^{\mathrm{EBH}} + [\mathcal{U}, K_B^{\mathrm{EBH}}] + (1/2!)[\mathcal{U},[\mathcal{U},K_B^{\mathrm{EBH}}]] + \cdots$, with

$$\mathcal{U} = \frac{1}{\sqrt{S}}\sum_{\mathbf{q},i}[e^{i\mathbf{q}\cdot\mathbf{R}_i}\alpha_{\mathbf{q},i}^*\hat{a}_{\mathbf{q}}^\dagger - e^{-i\mathbf{q}\cdot\mathbf{R}_i}\alpha_{\mathbf{q},i}\hat{a}_{\mathbf{q}}]\hat{n}_j,$$

where the coefficients α of the transformation will be defined by using a variational method. Impurity and lattice-mode operators transform as

$$e^{-\mathcal{U}}\hat{b}_j e^{\mathcal{U}} = \hat{b}_j e^{\frac{1}{\sqrt{S}}\sum_{\mathbf{q}}(e^{-i\mathbf{q}\cdot\mathbf{R}_j}\alpha_{\mathbf{q},j}\hat{a}_{\mathbf{q}} - e^{i\mathbf{q}\cdot\mathbf{R}_j}\alpha_{\mathbf{q},j}^*\hat{a}_{\mathbf{q}}^\dagger)},$$
$$e^{-\mathcal{U}}\hat{a}_{\mathbf{q}}e^{\mathcal{U}} = \hat{a}_{\mathbf{q}} - \frac{1}{\sqrt{S}}\sum_j e^{i\mathbf{q}\cdot\mathbf{R}_j}\,\alpha_{\mathbf{q},j}^*\,\hat{n}_j. \tag{10}$$

By plugging Eq. (10) into Eq. (8), and by considering $\alpha_{\mathbf{q},j} = (g_{AB}\sqrt{n_A}/\epsilon_q)\Omega_{\mathbf{q}}^{jj}\exp(i\mathbf{q}\cdot\mathbf{R}_j)$, which was determined through the minimization of the total energy of the system (see Appendix B), we obtain

$$\tilde{K}_B = -\tilde{J}\sum_{\langle i,j\rangle}\hat{b}_i^\dagger\hat{b}_j + \frac{\tilde{U}}{2}\sum_i\hat{n}_i(\hat{n}_i-1) - \tilde{\mu}\sum_i\hat{n}_i - \frac{V}{2}\sum_{\langle i,j\rangle}\hat{n}_i\hat{n}_j - P\sum_{\langle i,j\rangle}(\hat{n}_i+\hat{n}_j)\hat{b}_i^\dagger\hat{b}_j. \tag{11}$$

The coefficients read (see Appendix A)

$$\tilde{J} = Jf^0, \tag{12}$$

$$\tilde{U} = U - 2\frac{g_{AB}^2n_A}{S}\sum_{\mathbf{q}}\frac{|\Omega_{\mathbf{q}}^{ii}|^2}{\epsilon_{\mathbf{q}}}, \tag{13}$$

$$\tilde{\mu} = \mu_B + \frac{g_{AB}^2n_A}{S}\sum_{\mathbf{q}}\frac{|\Omega_{\mathbf{q}}^{ii}|^2}{\epsilon_{\mathbf{q}}}, \tag{14}$$

$$V = 2\frac{g_{AB}^2n_A}{S}\sum_{\mathbf{q}}\frac{|\Omega_{\mathbf{q}}^{ii}|^2e^{-i\mathbf{q}\cdot\mathbf{d}}}{\epsilon_{\mathbf{q}}}, \tag{15}$$

$$P = \frac{g_{AB}^2n_A}{S}\sum_{\mathbf{q}}\frac{1}{\epsilon_{\mathbf{q}}}\left(\Omega_{\mathbf{q}}^{ij}\Omega_{\mathbf{q}}^{ii*} + \bar{\Omega}_{\mathbf{q}}^{ij}\Omega_{\mathbf{q}}^{ii}\right)f^0, \tag{16}$$

where

$$f^0 = \exp\left\{-\frac{g_{AB}^2n_A}{2S}\sum_{\mathbf{q}}\frac{|\Omega_{\mathbf{q}}^{ii}|^2}{\epsilon_{\mathbf{q}}^2}|1-e^{-i\mathbf{q}\cdot\mathbf{d}}|^2\right\}. \tag{17}$$

Vortex-lattice fluctuations induce the appearance of additional terms in the effective impurity Hamiltonian [cf. difference between Eqs. (4) and (11)]. An estimate of V and P for typical values of the physical parameters is reported in Appendix D. The long-range interaction between impurities located at

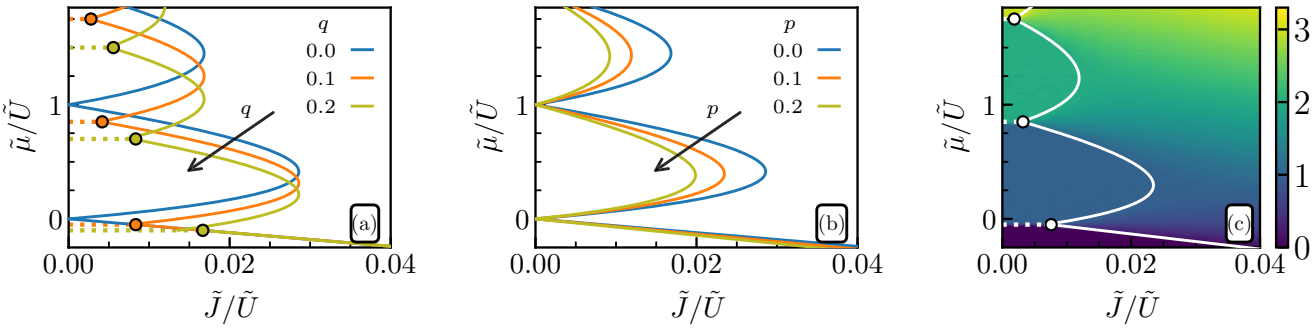

FIG. 1. Phase diagram of the EBH model in Eq. (11), featuring continuous MI/SF transitions (solid lines) and discontinuous MI/MI transitions (dashed lines). We show the separate effects of the long-range attraction q [panel (a), with $p = 0$] and of the density-dependent hopping p [panel (b), with $q = 0$], where the triple point and the MI/SF boundaries are computed through Eqs. (24) and (33), respectively. (c) Density $\langle \hat{n}_i \rangle$ for $q = p = 0.1$, computed through the Gutzwiller method (color codes, with $n_{\max} = 6$), compared with the analytical phase boundaries.

different sites occurs by means of the Tkachenko-mode scattering. One can show that this interaction decays rapidly with the intervortex distance, so that we can restrict the potential range to pairs of nearest-neighboring sites. Moreover, the Hamiltonian includes a density-dependent hopping, with amplitude P, which was not considered in Ref. [23]. Also in this case, we shall neglect processes between sites at distances larger than one lattice constant.

III. EXTENDED BOSE-HUBBARD PHASE DIAGRAM

In this section we determine the ground-state phase diagram of the EBH model in Eq. (11) through two methods. The Gutzwiller variational approach allows us to numerically compute relevant observables in the whole phase diagram, to identify the Mott and superfluid regions. By truncating the number of variational parameters, we also extract analytical expressions for the triple-point position and MI/SF phase boundary. Furthermore, we compute the MI/SF boundary through a mean-field approach, and the two methods agree with each other to high accuracy.

We introduce the dimensionless parameters

$$q = \frac{zV}{\tilde{U}}, \quad p = \frac{P}{\tilde{J}}, \tag{18}$$

and define z as the number of nearest neighbors of each site ($z = 6$, for the triangular lattice). Our results are shown in Fig. 1, where we observe several features: (i) In the $p = 0$ phase diagram [cf. Fig. 1(a)], the position and size of the MI lobes is modified due to $q > 0$, and their boundaries at $\tilde{J} = 0$ are given by

$$\frac{\tilde{\mu}^{g,g+1}}{\tilde{U}} = g - \frac{2g+1}{2} q, \tag{19}$$

for MI lobes with filling g and $g + 1$. This effect was also described in Ref. [23], and the boundary between MI lobes at $\tilde{J} = 0$ [Eq. (19)] is reproduced both with approximate methods (in the current work) and in the exact quantum Monte Carlo phase diagram [23]. (ii) The boundary between two subsequent MI regions is not restricted to one point at $\tilde{J} = 0$, but it extends up to a triple point at $\tilde{J} > 0$ [cf. Fig. 1(a)]. (iii) A nonzero value of p reduces the area of the MI regions [cf. Fig. 1(b)], which follows from the fact that p contributes as an additional part of the hopping term. Within the MF treatment, the value of $\tilde{J}/\tilde{U}$ for the $g = 1$ MI lobe tip is decreased by 8% when $p = 0.04$ (a realistic value for experiments; see Appendix D), and by 18% when $p = 0.1$.

A. Gutzwiller ansatz

The Gutzwiller variational ansatz [5,42,43] is a standard tool to treat bosonic lattice systems, giving access to both static and dynamic properties of the BH model. In the homogeneous version that we employ in this work, the ansatz for the wave function reads

$$|G\rangle = \prod_i \sum_{n=0}^{n_{\max}} f_n |n\rangle_i, \tag{20}$$

where the product runs over all lattice sites. The coefficients f_n of the on-site Fock states $|n\rangle_i$ do not depend on the lattice site i, and $n_{\max}$ is a cutoff on the maximum on-site occupation number. Writing the ground state of $\tilde{K}_B$ as a product of single-site states is only valid as an approximation. For the ordinary Bose-Hubbard model (with $V = P = 0$), this approximation becomes exact both in the $\tilde{U} \to 0$ and $\tilde{J} \to 0$ limits [2] (in the infinite-volume limit and with $n_{\max} \to \infty$).

We use $|G\rangle$ as a variational ansatz for the ground state of $\tilde{K}_B$, which depends on the $n_{\max} + 1$ variational parameters $\{f_n\}$. To extract observables from this ansatz, one should first find the set of coefficients $\{f_n\}$ that minimizes the expectation value of the energy per site, $\mathcal{E}(f_0, \ldots, f_{n_{\max}})$. We perform the optimization numerically through Simulated Annealing [44], which is a stochastic minimization algorithm (an implementation is made publicly available [45]).

For the ordinary BH model, the optimization of the Gutzwiller ansatz is strictly equivalent to the MF theory based on the decoupling [46]

$$\hat{b}_i^\dagger \hat{b}_j \simeq \varphi^* \hat{b}_j + \hat{b}_i^\dagger \varphi - |\varphi|^2, \tag{21}$$

where $\varphi \equiv \langle \hat{b}_i \rangle$ is the condensate order parameter, assumed to be independent of the site i. The choice of the decoupling is less straightforward when the Hamiltonian includes additional terms, as we mention in Sec. III B. The Gutzwiller variational procedure, however, remains well defined, so that we use it as the basis of our analysis. Once the optimal set of coefficients

$\{f_n\}$ is found, several observables can be computed, and especially the density $\langle \hat{n}_i \rangle$ and the condensate density $|\varphi|^2$. As an example (for a specific choice of V and P), the density as a function of $\tilde{J}/\tilde{U}$ and $\tilde{\mu}/\tilde{U}$ is shown in Fig. 1(c), where we identify the Mott lobes with integer density. These regions corresponds to those where the condensate density vanishes (not shown).

For $q > 0$, the boundary between two subsequent Mott lobes is defined on a finite $\tilde{J}$ interval at $\tilde{\mu} = \tilde{\mu}^{g,g+1}$, extending up to a triple point [where $\tilde{J}/\tilde{U}$ equals $(\tilde{J}/\tilde{U})^{g,g+1}_{\text{triple}}$], and it is characterized by a discontinuous jump in the density. Three transition lines cross at the triple point: the MI/SF transition for the gth Mott lobe, the MI/SF transition for the $(g+1)$th Mott lobe, and the MI/MI transition between the gth and $(g+1)$th Mott lobes (see Fig. 1).

To locate the triple point, we simplify the Gutzwiller ansatz, so that it can be treated analytically. Close to the transition between two subsequent Mott phases with filling g and $g+1$, it is a valid approximation to only consider the two on-site Fock states $|g\rangle$ and $|g+1\rangle$, which results in the ansatz

$$|G_2\rangle = \prod_i [\cos\theta |g\rangle_i + \sin\theta |g+1\rangle_i], \tag{22}$$

where θ is the only variational parameter. For $\theta = 0$ and $\theta = \pi/2$, this state corresponds to a product of local Fock states with filling equal to g and $g+1$, respectively. This corresponds to a MI state. When $0 < \theta < \pi/2$, on the contrary, each local state is mixed, and the average value of $\hat{b}_i$,

$$\langle \hat{b}_i \rangle \equiv \cos\theta \sin\theta \sqrt{g+1}, \tag{23}$$

takes a nonzero value, which corresponds to a SF state [within the approximation in Eq. (22)]. As in the more general case of $|G\rangle$, the variational approach requires finding the value of θ which minimizes the average energy per site $\mathcal{E}(\theta)$. At the MI/MI transition, $\mathcal{E}(\theta)$ shows the double-well shape that is peculiar of discontinuous transitions, where an energy barrier separates two local minima with the same energy. If $\tilde{\mu}$ is slightly lower (higher) than $\tilde{\mu}^{g,g+1}$, the minimum in $\theta = 0$ ($\theta = \pi/2$) becomes the global minimum, and the ground state is a Mott insulator with g ($g+1$) atoms per site.

When the chemical potential is tuned to its boundary value ($\tilde{\mu} = \tilde{\mu}^{g,g+1}$), the energy profile is symmetric: $\mathcal{E}(\theta) = \mathcal{E}(\pi/2 - \theta)$, and the height of the energy barrier between the two minima equals $\Delta\mathcal{E} = \mathcal{E}(\pi/4) - \mathcal{E}(0)$. This barrier height decreases when $\tilde{J}/\tilde{U}$ increases, and the triple point is reached when $\Delta\mathcal{E} = 0$. This condition can be explicitly rewritten as

$$\left(\frac{z\tilde{J}}{\tilde{U}}\right)^{g,g+1}_{\text{triple}} = \frac{q}{2(1+g)(1+p+2pg)}. \tag{24}$$

When $\tilde{J}/\tilde{U}$ increases beyond the triple point, the minimum of $\mathcal{E}$ takes place at a finite value of the variational parameter θ, corresponding to the SF phase. The triple point in Eq. (24), computed within the two-states Gutzwiller ansatz, agrees with the values found via the numerical data obtained with the full Gutzwiller scheme; see Fig. 1(c).

The MI/SF phase transition is characterized by number fluctuations and the two-states approximation $|G_2\rangle$ is not sufficient to identify the corresponding boundaries away from the triple point. To this purpose, we consider the three-states ansatz

$$|G_3\rangle = \prod_i [\cos\theta_1 \sin\theta_2 |g-1\rangle_i + \cos\theta_1 \cos\theta_2 |g\rangle_i + \sin\theta_1 |g+1\rangle_i], \tag{25}$$

where θ_1 and θ_2 are variational parameters. In the gth Mott lobe one has $\theta_1 = \theta_2 = 0$. To the lowest order in powers of θ_1 and θ_2, the energy per site corresponding to the ansatz (25) is

$$\mathcal{E}(\theta_1,\theta_2) = \mathcal{E}_0 + \sum_{a,b=1,2} \theta_a M_{ab} \theta_b, \tag{26}$$

where

$$\begin{aligned}
\mathcal{E}_0 &= g(g-1)\frac{\tilde{U}}{2} - \frac{g^2 z V}{2} - g\tilde{\mu}, \\
M_{11} &= g\tilde{U} - (g+1)z\tilde{J} - (2g^2+3g+1)zP - gzV - \tilde{\mu}, \\
M_{22} &= (1-g)\tilde{U} - gz\tilde{J} - g(2g-1)zP + gzV + \tilde{\mu}, \\
M_{12} &= M_{21} = -\sqrt{g(g+1)}z\tilde{J} - 2g\sqrt{g(g+1)}zP.
\end{aligned} \tag{27}$$

The phase boundaries are then obtained through the saddle point condition, namely by solving $\det M = 0$ (out of the two solutions, the one with smallest $\tilde{J}$ should be considered). The resulting analytical expression for the transition lines matches with the numerical phase diagram computed through the Gutzwiller ansatz. In particular, the tip of the lobe is located at the critical value

$$\left(\frac{z\tilde{J}}{\tilde{U}}\right)_c = \frac{1}{p + (1+2gp)[2g+1+2\sqrt{g(g+1)}]}. \tag{28}$$

This value depends on p, and the effect is larger for MI regions with larger filling g [47]. We stress that the nearest-neighbor attraction q, on the contrary, only affects the position of the lobe tip along the chemical-potential axis, and not the value of $(z\tilde{J}/\tilde{U})_c$.

B. Mean-field theory

Following the conventional approach used for the BH model, we also compute the phase diagram through a perturbative MF analysis [4–6] (an alternative approach is described in Appendix E). Similarly to Eq. (21), we decouple the density-dependent hopping term as

$$\hat{b}_i^\dagger \hat{n}_i \hat{b}_j \simeq \varphi \hat{b}_i^\dagger \hat{n}_i + \varphi \hat{n}_i \hat{b}_j - \varphi^2 \hat{n}_i, \tag{29}$$

assuming that φ is real. This allows us to write the Hamiltonian in Eq. (11) as $\tilde{K}_B = \tilde{K}_B^{(0)} + \varphi \tilde{K}_B^{(1)}$, with

$$\tilde{K}_B^{(0)} = \frac{\tilde{U}}{2}\sum_i \hat{n}_i(\hat{n}_i - 1) - \tilde{\mu}\sum_i \hat{n}_i - \frac{V}{2}\sum_{\langle i,j\rangle} \hat{n}_i \hat{n}_j + z\tilde{J}\varphi^2 \left[N_s(1+p) + 2p\sum_i \hat{n}_i \right] \tag{30}$$

and

$$\tilde{K}_B^{(1)} = -z\tilde{J}\sum_i \{[1+p(\hat{n}_i+1)]\hat{b}_i + \hat{b}_i^\dagger[1+p(\hat{n}_i+1)]\} - p\tilde{J}\sum_{\langle i,j\rangle}(\hat{n}_i\hat{b}_j + \hat{b}_i^\dagger \hat{n}_j), \tag{31}$$

with N_s being the number of sites. $\tilde{K}_B^{(0)}$ is diagonal in the Fock basis, while $\tilde{K}_B^{(1)}$ only includes off-diagonal terms. Due to the presence of nearest-neighbor interactions and density-dependent hopping, neither $\tilde{K}_B^{(0)}$ nor $\tilde{K}_B^{(1)}$ are defined on a single site, at a difference with the ordinary MF theory for the BH model. To identify the MI/SF transition, we study the stability of the homogeneous Fock state $|\Phi_g\rangle = |g,\ldots,g\rangle$, by treating $\varphi\tilde{K}_B^{(1)}$ as a perturbative correction. For $\tilde{J}=0$, φ vanishes and the unperturbed ground state is $|\Phi_g\rangle$, for $\tilde{\mu}^{g-1,g} < \tilde{\mu} < \tilde{\mu}^{g,g+1}$ [23]. We compute the total energy at second order in perturbation theory [6], $E(g) = E_0(g) + \varphi^2 E_2(g)$, as

$$E_2(g) = \sum_k \sum_{\alpha=P,H} \frac{\left|\langle\Phi_g|\tilde{K}_B^{(1)}|\Phi_g^{k,(\alpha)}\rangle\right|^2}{E_0(g) - E_0^{(\alpha)}(g)}, \tag{32}$$

considering the following excited states with an additional particle (P) or hole (H) on site k: $|\Phi_g^{k,(P)}\rangle = \frac{\hat{b}_k^\dagger}{\sqrt{g+1}}|\Phi_g\rangle$ and $|\Phi_g^{k,(H)}\rangle = \frac{\hat{b}_k}{\sqrt{g}}|\Phi_g\rangle$. The energy of the unperturbed state reads $E_0(g) = N_s\mathcal{E}_0 + z\tilde{J}\varphi^2 N_s(1+p+2pg)$ [see Eq. (27)].

The MI lobe boundary corresponds to the condition that the coefficient of φ^2 in $E(g)$ vanishes, which yields

$$\frac{z\tilde{J}}{\tilde{U}} = [1+p(2g+1)]\left[\frac{(g+1)[1+p(2g+1)]^2}{\Delta\mathcal{E}_P} + \frac{g(1+2pg)^2}{\Delta\mathcal{E}_H}\right]^{-1}, \tag{33}$$

where the energy gaps

$$\Delta\mathcal{E}_P = \tilde{U}g - \tilde{\mu} - zVg, \tag{34}$$

$$\Delta\mathcal{E}_H = -\tilde{U}(g-1) + \tilde{\mu} + zVg \tag{35}$$

are associated with single-site particle/hole excitations at $\tilde{J}=0$.

By comparing the MF analytical phase diagram with the one obtained through the $|G_3\rangle$ Gutzwiller ansatz, we find that the two approaches are essentially equivalent. As an example, we consider the value of $\tilde{J}/\tilde{U}$ at the tip of the $g=1$ lobe [extracted from Eq. (33)] and compare it with the Gutzwiller result in Eq. (28): For p as large as 0.3, the relative deviation is as small as 0.5%, and the difference becomes even smaller when lobes with larger g are considered.

IV. CONCLUSIONS

We determined the quantum phase diagram of ultracold bosonic impurities immersed in a vortex lattice. The effective EBH model (derived via the polaron transformation, with parameters chosen through the variational method), takes into account the lattice excitations represented by Tkachenko modes. These excitations generate peculiar terms in the resulting EBH model, namely a long-range attractive potential and a density-dependent hopping. The corresponding coefficients V and P are enhanced, as compared to ordinary optical-lattice realizations of the Bose-Hubbard model. The phase diagram includes Mott-insulator and superfluid phases, and it is computed with two independent techniques (a Gutzwiller variational approach and a perturbative mean-field theory). The separate effects of V and P on the MI lobes are clearly identified: A nonvanishing V leads to the appearance of discontinuous MI/MI transitions and of a triple point, while a nonzero P induces a shift of the critical hopping parameter for the SF/MI transition. The triple point can also be recognized in the exact phase diagram of the model for $P=0$, previously computed through the quantum Monte Carlo technique [23].

For the experimental realization of our scheme, we propose to employ the technique of artificial magnetic fields [29], for which the generation of vortices is currently being optimized [31] and could potentially reach the vortex-lattice regime predicted by theory [29,32]. Finally, although we focused here on neutral bosons, the atomic trapped species could also consist of fermions with spin charges, which would allow one to study magnetism with ultracold atoms, including triangular-lattice frustrated spins.

ACKNOWLEDGMENTS

We acknowledge Chiara Menotti and Elia Macaluso for useful discussions. This work is supported by CAPES/PROEX, FAPESP/CEPID, the EU-FET Proactive grant AQuS, Project No. 640800, ERC Starting Grant TopoCold, and by Provincia Autonoma di Trento.

APPENDIX A: EFFECTIVE EBH MODEL

The EBH in Eq. (11) results from the unitary transformation in the Hamiltonian of Eq. (8), followed by its average over the lattice modes, i.e., $\tilde{K}_B = \langle\tilde{K}_B\rangle_{\rm ph}$, with $|{\rm ph}\rangle = \prod_{\mathbf{q}}|N_{\mathbf{q}}\rangle$ and $|N_{\mathbf{q}}\rangle$ being the number state of the lattice modes [48, Secs. 4.31 and 4.32]. From that, we obtain the energy coefficients

$$\begin{aligned}
\tilde{U} &= U + \frac{2}{S}\sum_{\mathbf{q}}\left[|\alpha_{i,\mathbf{q}}|^2\epsilon_{\mathbf{q}} - g_{AB}\sqrt{n_A}\left(\Omega_{\mathbf{q}}^{ii}e^{i\mathbf{q}\cdot\mathbf{R}_i}\alpha_{i,\mathbf{q}}^* + \Omega_{\mathbf{q}}^{ii*}e^{-i\mathbf{q}\cdot\mathbf{R}_i}\alpha_{i,\mathbf{q}}\right)\right],\\
\tilde{\mu} &= \mu_B - \frac{1}{S}\sum_{\mathbf{q}}\left[|\alpha_{i,\mathbf{q}}|^2\epsilon_{\mathbf{q}} - g_{AB}\sqrt{n_A}\left(\Omega_{\mathbf{q}}^{ii}e^{i\mathbf{q}\cdot\mathbf{R}_i}\alpha_{i,\mathbf{q}}^* + \Omega_{\mathbf{q}}^{ii*}e^{-i\mathbf{q}\cdot\mathbf{R}_i}\alpha_{i,\mathbf{q}}\right)\right],\\
V &= -\frac{2}{S}\sum_{\mathbf{q}}\left[\alpha_{j,\mathbf{q}}^*\alpha_{i,\mathbf{q}}e^{-i\mathbf{q}\cdot\mathbf{d}}\epsilon_{\mathbf{q}} - g_{AB}\sqrt{n_A}\left(\Omega_{\mathbf{q}}^{jj}e^{i\mathbf{q}\cdot\mathbf{R}_i}\alpha_{i,\mathbf{q}}^* + \Omega_{\mathbf{q}}^{jj*}e^{-i\mathbf{q}\cdot\mathbf{R}_i}\alpha_{i,\mathbf{q}}\right)\right],
\end{aligned} \tag{A1}$$

$$\begin{aligned}
\tilde{J} &= Jf^0,\\
P &= \frac{g_{AB}\sqrt{n_A}}{S}\sum_{\mathbf{q}}\left[\Omega_{\mathbf{q}}^{ij}e^{i\mathbf{q}\cdot\mathbf{R}_i}\alpha_{i,\mathbf{q}}^* + \bar{\Omega}_{\mathbf{q}}^{ij}e^{-i\mathbf{q}\cdot\mathbf{R}_i}\alpha_{i,\mathbf{q}}\right]f^0,
\end{aligned} \tag{A2}$$

which depend explicitly on the parameter α of the unitary transformation, including

$$f^0 = \exp\left[-\frac{1}{2S}\sum_{\mathbf{q}}|\alpha_{i\mathbf{q}}|^2|1-e^{-i\mathbf{q}\cdot\mathbf{d}}|^2\right]. \tag{A3}$$

Using the parameter α obtained through the variational method (see Appendix B), the energies above are reduced to Eqs. (12)–(16) in the main text.

APPENDIX B: VARIATIONAL METHOD

Applying the extremization condition to the total energy of the system, $E = \langle \tilde{K}_B\rangle_\Phi$, with $|\Phi_g\rangle = |g,\ldots,g\rangle$, we get

$$\frac{\partial E}{\partial \alpha_{i,\mathbf{q}}} \quad \text{implying} \quad \frac{\partial \mathcal{E}_0}{\partial \alpha_{i,\mathbf{q}}} = 0. \tag{B1}$$

The second condition is justified by using the fact that $P \sim \tilde{J}$ and $V \sim \tilde{U}$. Since $U \gg J$, only the ground-state energy is relevant. Applying Eq. (B1) to each element of the ground-state energy in Eq. (27), according to Eq. (A1)

$$\begin{aligned}
\frac{\partial \tilde{U}}{\partial \alpha_{i,\mathbf{q}}} &= \frac{2}{S}\left[\alpha^*_{i,\mathbf{q}}\epsilon_{\mathbf{q}} - g_{AB}\sqrt{n_A}\Omega^{ii*}_{\mathbf{q}}e^{-i\mathbf{q}\cdot\mathbf{R}_i}\right],\\
\frac{\partial \tilde{\mu}}{\partial \alpha_{i,\mathbf{q}}} &= -\frac{2}{S}\left[\alpha^*_{i\mathbf{q}}\epsilon_{\mathbf{q}} - g_{AB}\sqrt{n_A}\Omega^{ii*}_{\mathbf{q}}e^{-i\mathbf{q}\cdot\mathbf{R}_i}\right],\\
\frac{\partial V}{\partial \alpha_{i,\mathbf{q}}} &= -\frac{2}{S}\left[\alpha^*_{j,\mathbf{q}}\epsilon_{\mathbf{q}}e^{-i\mathbf{q}\cdot\mathbf{d}} - g_{AB}\sqrt{n_A}\Omega^{jj*}_{\mathbf{q}}e^{-i\mathbf{q}\cdot\mathbf{R}_i}\right].
\end{aligned} \tag{B2}$$

Assuming homogeneity ($\alpha_{i\mathbf{q}} \equiv \alpha_{j\mathbf{q}}$), we find

$$\alpha_{i,\mathbf{q}} = \frac{g_{AB}\sqrt{n_A}}{\epsilon_{\mathbf{q}}}\Omega^{ii}_{\mathbf{q}}e^{i\mathbf{q}\cdot\mathbf{R}_i}, \tag{B3}$$

which depends on the Tkachenko-mode parameters $\Omega^{ii}_{\mathbf{q}}$ and $\epsilon_{\mathbf{q}}$.

APPENDIX C: DENSITY-DEPENDENT HOPPING

In Ref. [16], the authors determined a generalized BH model by considering the nearest-neighbor contribution in the interacting term. For ultracold atoms trapped in a three-dimensional optical lattice, this reads

$$H = -J\sum_{\langle i,j\rangle}\hat{b}^\dagger_i\hat{b}_j + \frac{1}{2}\sum_{ijkl}U_{ijkl}\hat{b}^\dagger_i\hat{b}^\dagger_j\hat{b}_k\hat{b}_l - \mu\sum_i\hat{n}_i, \tag{C1}$$

with the total hopping

$$J_{\text{Total}} = \int d^3r\,\omega^*(\mathbf{r}_i)\left[-\frac{\hbar^2\nabla^2}{2m} + V(\mathbf{r}) + g\rho(\mathbf{r})\right]\omega^*(\mathbf{r}_j),$$

$$\text{with} \quad \rho = n_i|\omega(\mathbf{r}_i)|^2 + (n_j-1)|\omega(\mathbf{r}_j)|^2, \tag{C2}$$

and the long-range potential

$$V = g\int d^3r|\omega(\mathbf{r}_i)|^2|\omega(\mathbf{r}_j)|^2, \tag{C3}$$

where $g = 4\pi\hbar a_s/m$ is the repulsive contact potential and a_s the scattering length. We consider the hopping correction due to the interaction (in our two-dimensional case $g \equiv g_B$) $J_E = g_B\int d^2r\omega^*(\mathbf{r}_i)\rho(\mathbf{r})\omega^*(\mathbf{r}_j)$. By applying the Gaussian ansatz for the Wannier functions, $\omega_B(\mathbf{r}) = |B_0|e^{-r^2/2l_0^2}$, with width $l_0^2 = \hbar\xi_A/\sqrt{m_B V_0}$ (which corresponds to the harmonic ansatz for the vortex-core density profile [49, Chap. 9]), we derive

$$\begin{aligned}
J_E &= g_B(n_i+n_j-1)|B_0|^4\left\{\int_{-\infty}^{\infty}dx\exp\left[-(x-x_i)^2/2l_0^2 - (x-x_j)^2/2l_0^2 - (x-x_i)^2/l_0^2\right]\right\}^2\\
&= (n_i+n_j-1)\frac{g_B}{2\pi l_0^2}e^{-3d^2/4l_0^2} = (n_i+n_j-1)Ue^{-6\sqrt{2}\Gamma_L\sqrt{V_0/E_R}}
\end{aligned} \tag{C4}$$

and

$$\begin{aligned}
V_E &= g_B|B_0|^4\left\{\int_{-\infty}^{\infty}dx\exp\left[-(x-x_i)^2/l_0^2 - (x-x_j)^2/l_0^2\right]\right\}^2 = \frac{g_B}{2\pi l_0^2}e^{-d^2/l_0^2}\\
&= Ue^{-8\sqrt{2}\Gamma_L\sqrt{V_0/E_R}},
\end{aligned} \tag{C5}$$

where $d = x_i - x_j$, $U_{iiij} = J_E$, and $U_{ijij} = V_E$.

In addition, we determine the on-site energy, $U = E_R(2/\sqrt{\pi})(a_B/l_z^B)\sqrt{V_0/E_R}$, and the hopping, $J = E_R[(2\Gamma_L-1)(V_0/E_R) - (\sqrt{2}/4)\sqrt{V_0/E_R}]e^{-2\sqrt{2}\Gamma_L\sqrt{V_0/E_R}}$. By comparing the magnitude of the different terms in Fig. 2, it is clear that the off-site energies decay faster than U and J. This analysis justifies the validity of the BH truncation applied in Eq. (4).

On the other hand, by applying the same procedure for the effective EBH in Eq. (11), where we associate the hopping

$$\hat{\tilde{J}}_{\text{Total}} = \hat{\tilde{J}} + \hat{J}_P \tag{C6}$$

with $\hat{\tilde{J}} = -\tilde{J}\hat{b}^\dagger_i\hat{b}_j$, $\hat{J}_P = -P(\hat{n}_j+\hat{n}_i)\hat{b}^\dagger_i\hat{b}_j$, and $\tilde{J} = Jf^0$, we find

$$\hat{\tilde{J}}_{\text{Total}} = -[Jf^0 + P(\hat{n}_j+\hat{n}_i)]\hat{b}^\dagger_i\hat{b}_j. \tag{C7}$$

Finally, using the "bare" hopping from Eq. (5) and the explicit form of the density-dependent hopping P given by

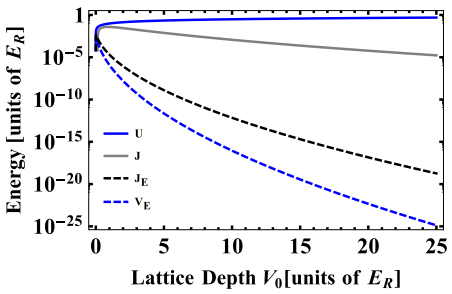

FIG. 2. From top to bottom: Solid blue: on-site energy U. Solid gray: "Gaussian" hopping J. Dashed black: induced hopping J_E. Dashed blue: long-range potential V_E. We set $a_B/l_z^B \approx 0.05$ with $\Gamma_L \approx 1$ for ^{87}Rb atoms and assume a unitary filling of the lattice sites, $n_i = n_j = 1$.

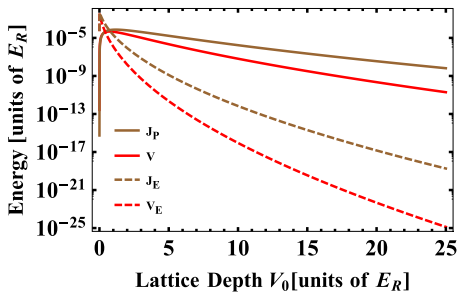

FIG. 3. From top to bottom: Solid brown: "dynamic" hopping J_P. Solid red: long-range potential V. Dashed brown: "static" induced hopping J_E. Dashed red: long-range "static" potential V_E. We use the mixture Na-Rb, where Rb atoms are considered as impurities. In addition, we assume a unitary filling of the lattice sites ($n_i = n_j = 1$) and $\Gamma_L \approx 1$.

Eq. (16), we obtain

$$\hat{\tilde{J}}_{\text{Total}} = f^0 \int d^2 r \omega^*(\mathbf{r}_i)\left[-\frac{\hbar^2\nabla^2}{2m_B} + \hat{V}_{\text{eff}}\right]\omega(\mathbf{r}_j)\hat{b}_i^\dagger \hat{b}_j, \quad \text{(C8)}$$

with $\hat{V}_{\text{eff}} = V_{AB}(\mathbf{r}) - V_0\hat{\rho}(\mathbf{r})$ and $\hat{\rho}(\mathbf{r}) = \mathcal{X}(\mathbf{r})(\hat{n}_j + \hat{n}_i)$ being the effective potential associated with density-dependent hopping and reduced density, respectively. The parameter $\mathcal{X}(\mathbf{r}) = (g_{AB}/S)\sum_{\mathbf{q}}[(\varphi_A u_{\mathbf{q}}^* - \varphi_A^* v_{\mathbf{q}})\Omega_{\mathbf{q}}^{ii} + \text{c.c.}](1/\epsilon_{\mathbf{q}})$ represents the impurity spatial density "dressed" by the lattice modes, with $\Omega_{\mathbf{q}}^{ii}$ given by Eq. (9).

APPENDIX D: EBH PARAMETERS IN THE CONTINUUM LIMIT

The dispersion relation of the Tkachenko modes in the continuum limit is established by considering small values of momentum, that is, $ql \ll 1$ [36]. In addition, we consider the energy dispersion of the Tkachenko modes $\epsilon_q \approx \hbar^2 q^2/2M$, with $M = \frac{1}{2\kappa\sqrt{\eta}}\frac{\hbar\Omega}{n_A g_A} m_A$ being the effective mass of the modes and the lattice constants $\kappa = 1.1592$ and $\eta = 0.8219$. In the low-energy limit, we have $u_{\mathbf{q}}(\mathbf{r}) \approx \varphi_A(\mathbf{r}) c_{1\mathbf{q}}\, e^{i\mathbf{q}\cdot\mathbf{r}}$ and $v_{\mathbf{q}}(\mathbf{r}) \approx \varphi_A(\mathbf{r}) c_{2\mathbf{q}}\, e^{-i\mathbf{q}\cdot\mathbf{r}}$. The small value of the momentum allows us to expand $(c_{1q} - c_{2q}) \approx \frac{1}{\sqrt{2}}\eta^{1/4}(ql)$. Using these considerations and the Gaussian ansatz for the Wannier functions (see Appendix C), we determine the Ω and $\bar{\Omega}$ in Eq. (9), which leads to

$$\begin{aligned}\left|\Omega_{\mathbf{q}}^{ii}\right|^2 &= \frac{\eta^{1/2}}{2}(ql)^2\left(\frac{|B_0|}{2\xi_A^2}\int d\mathbf{r} e^{\pm i\mathbf{q}\cdot\mathbf{r}} e^{-r^2/2l_0^2}\right)^2 \\ &= \frac{\eta^{1/2}}{128}(ql)^2\left(\frac{l_0^2}{\xi_A^2}\right)^2\left(4 - q^2 l_0^2\right)^2 e^{-q^2 l_0^2/2}, \end{aligned} \quad \text{(D1)}$$

where the sign $\pm$ is associated with $\Omega_{\mathbf{q}}^{ii}$ and $\bar{\Omega}_{\mathbf{q}}^{ii}$, respectively. In the same way, we obtain

$$\begin{aligned}\Omega_{\mathbf{q}}^{ij} &= \frac{\eta^{1/4}}{\sqrt{2}}(ql)\left(|B_0|\int d\mathbf{r} e^{\pm i\mathbf{q}\cdot\mathbf{r}} e^{-r^2/2l_0^2} e^{-|\mathbf{r}+\mathbf{d}|^2/2l_0^2}\right) \\ &= \frac{1}{\sqrt{2}}\eta^{1/4}(ql) e^{-d^2/4l_0^2} e^{-q^2 l_0^2/4} e^{-i\mathbf{q}\cdot\mathbf{d}/2}, \end{aligned} \quad \text{(D2)}$$

where, we find $\bar{\Omega}_{\mathbf{q}}^{ij} = \Omega_{\mathbf{q}}^{ij*}$ for the continuum case.

The long-range potential is obtained by substituting the above relations into Eq. (15):

$$\begin{aligned} V &= \frac{2g_{AB}^2 n_A}{S}\sum_{\mathbf{q}}\frac{1}{\epsilon_q} \\ &\quad\times\left[\frac{\eta^{1/2}}{128}(ql)^2\left(\frac{l_0^2}{\xi_A^2}\right)^2\left(4 - q^2 l_0^2\right)^2 e^{-q^2 l_0^2/2} e^{-i\mathbf{q}\cdot\mathbf{d}}\right] \\ &\sim \int d\mathbf{q}\left(4 - q^2 l_0^2\right)^2 e^{-q^2 l_0^2/2} e^{-i\mathbf{q}\cdot\mathbf{d}} \sim U e^{-d^2/2l_0^2} \\ &= U\gamma_1\left(\frac{V_0}{E_R}\right)\left(1 + 16\Gamma_L^2\frac{V_0}{E_R}\right) e^{-4\sqrt{2}\Gamma_L\sqrt{V_0/E_R}}, \end{aligned} \quad \text{(D3)}$$

where $\gamma_1 = (1/4\kappa)(m_A/m_B)^{3/2}(a_A/a_B)$.

The density-dependent hopping is determined by plugging relations (D1) and (D2) into Eq. (16):

$$\begin{aligned} P &= \frac{g_{AB}^2 n_A}{S}\sum_{\mathbf{q}}\frac{f^0}{\epsilon_q}\left[\frac{\eta^{1/4}}{\sqrt{2}}(ql)^2\left(\frac{l_0^2}{8\xi_A^2}\right)\left(4 - q^2 l_0^2\right)^2\right. \\ &\quad\left.\times e^{-q^2 l_0^2/4} e^{-d^2/4l_0^2}\cos(\mathbf{q}\cdot\mathbf{d}/2)\right] \\ &\sim f^0 e^{-d^2/4l_0^2}\int d\mathbf{q}\left(4 - q^2 l_0^2\right) e^{-q^2 l_0^2/2}\cos(\mathbf{q}\cdot\mathbf{d}/2) \\ &\sim f^0 U e^{-3d^2/8l_0^2} \\ &= \sqrt{2}U\gamma_1\left(\frac{V_0}{E_R}\right)^{3/2}\left(1 + \sqrt{2}\Gamma_L\sqrt{\frac{V_0}{E_R}}\right) e^{-(3\sqrt{2}+\gamma_2)\Gamma_L\sqrt{V_0/E_R}}, \end{aligned} \quad \text{(D4)}$$

where $\gamma_2 = (1/8\sqrt{\pi}\kappa^2\sqrt{\eta})(m_A^2/m_{AB}m_B)(a_A/l_z^B)$. Here we note, in both cases, that V and P decay with the intervortex distance d. f^0 is obtained in the same way as V and P. Following the MF approach of Ref. [16], we derive

$$J_P = (n_i + n_j)P. \quad \text{(D5)}$$

In Fig. 3, we compare the long-range potential and the induced-hopping for the "static" and "dynamic" case.

In order to determine numerical values of the long-range potential and density-dependent hopping, we consider the

mixture ^{23}Na and ^{87}Rb, where ^{23}Na ($m_A = 23u$) and ^{87}Rb ($m_B = 87u$) are the majority (A) and minority species (B), respectively, with $u \simeq 1.66 \times 10^{-27}$ kg being the atomic mass unit. For the sodium BEC, we assume an effective 2D atomic density of $n_A \approx (10^{20}/\mathrm{m}^3) \times l_z^A$ (with $l_z^A \sim 0.2$ μm), with $\omega_z \sim 2\pi \times 10$ kHz being the axial confinement and where the scattering length of species A is $a_A = 90a_0$ (with a_0 being the Bohr radius). This yields a unitary Landau factor $n_A g_A/2\hbar\Omega \sim 1$, the lattice parameter $d \sim 0.65$ μm, the vortex size $\xi_A \sim 0.3$ μm, and the Wannier-function length $l_0 \sim 0.2$ μm. With these parameter values, the tight-binding regime is satisfied: $V_0/E_R \sim 15 \gg 1$. Finally, we estimate the values for long-range potential and density-dependent hopping assuming reasonable values for the scattering lengths of species B, $a_B = 100a_0$, and for the interspecies scattering length $a_{AB} = 450a_0$. This allows us to be close to the MI/SF boundary, yielding $zV/\tilde{U} \sim 0.01$ ($z = 6$) and $P/\tilde{J} \sim 0.04$.

APPENDIX E: MEAN-FIELD PHASE BOUNDARIES

In this Appendix, we derive an alternative expression for the mean-field phase boundaries computed in Sec. III B, by applying the method developed for the dipolar EBH model [50]. On top of $\varphi_i = \langle \hat{b}_i \rangle$, we introduce the average on-site density $n_i = \langle \hat{n}_i \rangle$. Analogously to the decoupling in Eq. (21), we write the other off-site terms in Eq. (11) as

$$\begin{aligned}(\hat{n}_i + \hat{n}_j)\hat{b}_i^\dagger \hat{b}_j \approx{}& \varphi_j \hat{b}_i^\dagger \hat{n}_i + \varphi_i^* \hat{n}_j \hat{b}_j + \hat{b}_i^\dagger \varphi_j + \hat{b}_j \varphi_i^* - \varphi_i^* \varphi_j \\ &+ \varphi_j \hat{b}_i^\dagger \hat{n}_j + \varphi_i^* \hat{n}_i \hat{b}_j - \varphi_i^* \varphi_j (\hat{n}_i + \hat{n}_j), \\ \hat{n}_i \hat{n}_j \approx{}& n_j \hat{n}_i + n_i \hat{n}_j - n_i n_j. \end{aligned} \tag{E1}$$

In order to obtain a single-site Hamiltonian, we define $\varphi_i = \sum_{\langle i \rangle_j} \varphi_j$, $N_i = \sum_{\langle i \rangle_j} n_j$, and $\varphi_i \hat{n}_i = \sum_{\langle i \rangle_j} \varphi_j \hat{n}_j$, where the sums of φ_j and n_j over the nearest neighbors of site i. We also neglect terms which are of second order in φ_i; the Hamiltonian in Eq. (11) becomes $\tilde{K}_B = \tilde{K}_B^0 + \tilde{K}_B^1$, where

$$\begin{aligned}\tilde{K}_B^0 ={}& \sum_i \left[\frac{\tilde{U}}{2} \hat{n}_i (\hat{n}_i - 1) - \tilde{\mu} \hat{n}_i - \frac{V}{2} (2\hat{n}_i - n_i) N_i \right], \\ \tilde{K}_B^1 ={}& -\sum_i \{ [\tilde{J} + P(2\hat{n}_i + 1)] \hat{b}_i \varphi_i^* \\ &+ \hat{b}_i^\dagger \varphi_i [\tilde{J} + P(2\hat{n}_i + 1)] \}. \end{aligned} \tag{E2}$$

We consider $\tilde{K}_B^0$ as the main contribution to the ground-state energy and $\tilde{K}_B^1$ as a perturbation. This perturbative MF method identifies the region where a given density distribution $|\Psi\rangle = \prod_i |n_i\rangle$ is stable against particle and hole excitations, which corresponds to the Mott lobe. The method is formulated at finite temperature, followed by the zero-temperature limit. We assume that $|\Psi\rangle$ is a local minimum of $\tilde{K}_B^0$, with $\tilde{K}_B^0 |\Psi\rangle = E_0 |\Psi\rangle$ and

$$E_0 = \sum_i \mathcal{E}_0(n_i) = \sum_i \left[\frac{\tilde{U}}{2} n_i (n_i - 1) - \tilde{\mu} n_i - \frac{V}{2} n_i N_i \right]. \tag{E3}$$

At finite inverse temperature $\beta = 1/(k_B T)$ (where k_B is the Boltzmann constant), the order parameters φ_i can be obtained as $\varphi_i = \mathrm{Tr}[\hat{b}_i \hat{\rho}]$. The density matrix of the system is defined as $\hat{\rho} = e^{-\beta \tilde{K}_B}/Z$, with the partition function $Z = \mathrm{Tr}[e^{-\beta \tilde{K}_B}]$, which we approximate by the first term of the Dyson series: $Z \simeq \mathrm{Tr}[e^{-\beta E_0}]$. The Dyson expansion is also applied to calculate the order parameter, keeping only the lowest-order term and projecting it in the subspace formed by the states $|\gamma_1\rangle = |\Psi\rangle$ and $|\gamma_2\rangle = (\hat{b}_i/\sqrt{n_i})|\Psi\rangle$. Then, $\varphi_i = \mathrm{Tr}[\hat{b}_i e^{-\beta E_0} e^{-\beta \tilde{K}_B}]$ becomes

$$\varphi_i \approx -e^{\beta E_0} \int_0^\beta d\tau \sum_{|\gamma\rangle} \langle \gamma | \hat{b}_i e^{-(\beta-\tau)\tilde{K}_B^0} \tilde{K}_B^1 e^{-\tau \tilde{K}_B^0} | \gamma \rangle, \tag{E4}$$

$$\begin{aligned}\varphi_i &\approx e^{\beta E_0} \int_0^\beta d\tau \sum_{|\gamma\rangle = |\gamma_1\rangle}^{|\gamma_2\rangle} \langle \gamma | \hat{b}_i \sum_k e^{-(\beta-\tau)\tilde{K}_B^0} \left\{ [\tilde{J} + P(2\hat{n}_k + 1)] \hat{b}_k \varphi_k^* + \hat{b}_k^\dagger [\tilde{J} + P(2\hat{n}_k + 1)] \varphi_k \right\} e^{-\tau \tilde{K}_B^0} | \gamma \rangle \\ &\approx \varphi_i \left\{ (n_i + 1)[\tilde{J} + P(2n_i + 1)] \int_0^\beta d\tau e^{-(\beta-\tau)(E_+ - E_0)} + n_i [\tilde{J} + P(2n_i - 1)] \int_0^\beta d\tau e^{-\tau(E_- - E_0)} \right\}. \end{aligned} \tag{E5}$$

Taking the zero-temperature limit ($\beta \to \infty$), we derive the equation for the lobe boundaries

$$\varphi_i \approx \varphi_i \left[\frac{[\tilde{J} + P(2n_i + 1)](n_i + 1)}{E_+ - E_0} + \frac{[\tilde{J} + P(2n_i - 1)] n_i}{E_- - E_0} \right]. \tag{E6}$$

The energies are computed from $E_+ = \langle \gamma_3 | \tilde{K}_B^0 | \gamma_3 \rangle$ and $E_- = \langle \gamma_2 | \tilde{K}_B^0 | \gamma_2 \rangle$, with $|\gamma_3\rangle = (\hat{b}_i^\dagger/\sqrt{n_i + 1})|\Psi\rangle$. Then $E_+ - E_0 = \tilde{U} n_i - \tilde{\mu} n_i - V N_i$ and $E_- - E_0 = -\tilde{U}(n_i - 1) + \tilde{\mu} n_i + V N_i$. Using these relations, we obtain

$$\varphi_i \approx \varphi_i \left[\frac{[\tilde{J} + P(2n_i + 1)](n_i + 1)}{\tilde{U} n_i - \tilde{\mu} - V N_i} + \frac{[\tilde{J} + P(2n_i - 1)] n_i}{-\tilde{U}(n_i - 1) + \tilde{\mu} + V N_i} \right]. \tag{E7}$$

The validity of Eq. (E7) is restricted to the interval

$$\tilde{U}(n_i - 1) - V N_i \leqslant \tilde{\mu} \leqslant \tilde{U} n_i - V N_i. \tag{E8}$$

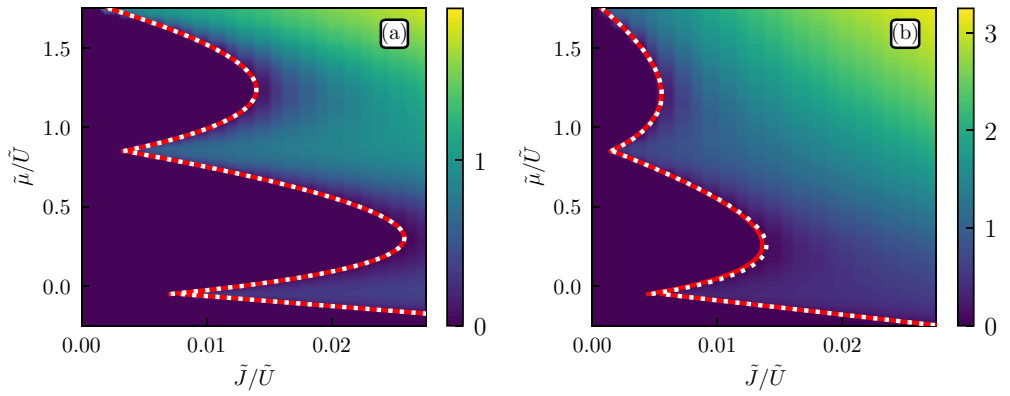

FIG. 4. Phase diagram of the EBH model at $q = 0.1$, with $p = 0.05$ (a) and $p = 0.5$ (b). The condensate density is computed through the Gutzwiller approach (color code, obtained with $n_{\max} = 6$). Also shown are the standard MF theory [solid red line, Eq. (33)] and the single-site MF approach [dotted white line, Eq. (E9)].

Considering the approximations $\varphi_i = z\varphi_i$ and $N_i = zn_i$, and assuming uniformity ($\varphi_i = \varphi$ and $n_i = g$), we rewrite the Eq. (E7) as

$$\frac{\tilde{U}}{z\tilde{J}} = \frac{[1 + p(2g + 1)](g + 1)}{g - \tilde{\mu}/\tilde{U} - qg} + \frac{[1 + p(2g - 1)]g}{-(g - 1) + \tilde{\mu}/\tilde{U} + qg}. \tag{E9}$$

From the expression for the lobe boundary, we can identify the critical point, that is, the tip of the lobe. This point satisfies

$$\left(\frac{z\tilde{J}}{\tilde{U}}\right)_c = [1 + p + 2g(1 + p + 2pg) + 2\sqrt{g(1 + g)[1 + p(2g + 1)][1 + p(2g - 1)]}]^{-1}. \tag{E10}$$

This alternative derivation for the lobe boundary provides results essentially equivalent to the other two approaches (the Gutzwiller ansatz and the standard MF method). The comparison is shown in Fig. 4, for both small and large values of p.

[1] I. Bloch, Ultracold quantum gases in optical lattices, Nat. Phys. **1**, 23 (2005).

[2] I. Bloch, J. Dalibard, and W. Zwerger, Many-body physics with ultracold gases, Rev. Mod. Phys. **80**, 885 (2008).

[3] M. Lewenstein, A. Sanpera, and V. Ahufinger, *Ultracold Atoms in Optical Lattices: Simulating Quantum Many-Body Systems* (Oxford University Press, Oxford, 2012).

[4] M. P. A. Fisher, P. B. Weichman, G. Grinstein, and D. S. Fisher, Boson localization and the superfluid-insulator transition, Phys. Rev. B **40**, 546 (1989).

[5] D. Jaksch, C. Bruder, J. I. Cirac, C. W. Gardiner, and P. Zoller, Cold Bosonic Atoms in Optical Lattices, Phys. Rev. Lett. **81**, 3108 (1998).

[6] D. van Oosten, P. van der Straten, and H. T. C. Stoof, Quantum phases in an optical lattice, Phys. Rev. A **63**, 053601 (2001).

[7] M. Greiner, O. Mandel, T. Esslinger, T. W. Hänsch, and I. Bloch, Quantum phase transition from a superfluid to a Mott insulator in a gas of ultracold atoms, Nature (London) **415**, 39 (2002).

[8] S. Baier, M. J. Mark, D. Petter, K. Aikawa, L. Chomaz, Z. Cai, M. Baranov, P. Zoller, and F. Ferlaino, Extended Bose-Hubbard models with ultracold magnetic atoms, Science **352**, 201 (2016).

[9] E. G. D. Torre, E. Berg, and E. Altman, Hidden Order in 1D Bose Insulators, Phys. Rev. Lett. **97**, 260401 (2006).

[10] T. Lahaye, C. Menotti, L. Santos, M. Lewenstein, and T. Pfau, The physics of dipolar bosonic quantum gases, Rep. Prog. Phys. **72**, 126401 (2009).

[11] C. Trefzger, C. Menotti, B. Capogrosso-Sansone, and M. Lewenstein, Ultracold dipolar gases in optical lattices, J. Phys. B: At. Mol. Phys. **44**, 193001 (2011).

[12] J. C. Amadon and J. E. Hirsch, Metallic ferromagnetism in a single-band model: Effect of band filling and Coulomb interactions, Phys. Rev. B **54**, 6364 (1996).

[13] J. E. Hirsch, Bond-charge repulsion and hole superconductivity, Phys. C (Amsterdam, Neth.) **158**, 326 (1989).

[14] J. E. Hirsch, Inapplicability of the Hubbard model for the description of real strongly correlated electrons, Physica B: Condens. Matter **199-200**, 366 (1994).

[15] O. Jürgensen, K. Sengstock, and D.-S. Lühmann, Density-induced processes in quantum gas mixtures in optical lattices, Phys. Rev. A **86**, 043623 (2012).

[16] D.-S. Lühmann, O. Jürgensen, and K. Sengstock, Multi-orbital and density-induced tunneling of bosons in optical lattices, New J. Phys. **14**, 033021 (2012).

[17] O. Jürgensen, F. Meinert, M. J. Mark, H.-C. Nägerl, and D.-S. Lühmann, Observation of Density-Induced Tunneling, Phys. Rev. Lett. **113**, 193003 (2014).

[18] Á. Rapp, X. Deng, and L. Santos, Ultracold Lattice Gases with Periodically Modulated Interactions, Phys. Rev. Lett. **109**, 203005 (2012).

[19] M. Di Liberto, C. E. Creffield, G. I. Japaridze, and C. M. Smith, Quantum simulation of correlated-hopping models with fermions in optical lattices, Phys. Rev. A **89**, 013624 (2014).

[20] F. Meinert, M. J. Mark, K. Lauber, A. J. Daley, and H.-C. Nägerl, Floquet Engineering of Correlated Tunneling in the Bose-Hubbard Model with Ultracold Atoms, Phys. Rev. Lett. **116**, 205301 (2016).

[21] F. Görg, M. Messer, K. Sandholzer, G. Jotzu, R. Desbuquois, and T. Esslinger, Enhancement and sign change of magnetic correlations in a driven quantum many-body system, Nature (London) **553**, 481 (2018).

[22] T. H. Johnson, Y. Yuan, W. Bao, S. R. Clark, C. Foot, and D. Jaksch, Hubbard Model for Atomic Impurities Bound by the Vortex Lattice of a Rotating Bose-Einstein Condensate, Phys. Rev. Lett. **116**, 240402 (2016).

[23] R. H. Chaviguri, T. Comparin, V. S. Bagnato, and M. A. Caracanhas, Phase transition of ultracold atoms immersed in a Bose-Einstein-condensate vortex lattice, Phys. Rev. A **95**, 053639 (2017).

[24] K. W. Madison, F. Chevy, W. Wohlleben, and J. Dalibard, Vortex Formation in a Stirred Bose-Einstein Condensate, Phys. Rev. Lett. **84**, 806 (2000).

[25] P. C. Haljan, I. Coddington, P. Engels, and E. A. Cornell, Driving Bose-Einstein-Condensate Vorticity with a Rotating Normal Cloud, Phys. Rev. Lett. **87**, 210403 (2001).

[26] J. R. Abo-Shaeer, C. Raman, J. M. Vogels, and W. Ketterle, Observation of vortex lattices in Bose-Einstein condensates, Science **292**, 476 (2001).

[27] V. K. Tkachenko, Elasticity of vortex lattices, Zh. Eksp. Teor. Fiz **56**, 1763 (1969) [J. Exp. Theor. Phys. **29**, 945 (1969)].

[28] I. Coddington, P. Engels, V. Schweikhard, and E. A. Cornell, Observation of Tkachenko Oscillations in Rapidly Rotating Bose-Einstein Condensates, Phys. Rev. Lett. **91**, 100402 (2003).

[29] I. B. Spielman, Raman processes and effective gauge potentials, Phys. Rev. A **79**, 063613 (2009).

[30] Y.-J. Lin, R. L. Compton, K. Jiménez-García, J. V. Porto, and I. B. Spielman, Synthetic magnetic fields for ultracold neutral atoms, Nature (London) **462**, 628 (2009).

[31] R. M. Price, D. Trypogeorgos, D. L. Campbell, A. Putra, A. Valdés-Curiel, and I. B. Spielman, Vortex nucleation in a Bose-Einstein condensate: From the inside out, New J. Phys. **18**, 113009 (2016).

[32] R. Bai, A. Roy, D. Angom, and P. Muruganandam, Condensates in double-well potential with synthetic gauge potentials and vortex seeding, arXiv:1705.06493.

[33] E. J. Mueller and T.-L. Ho, Two-Component Bose-Einstein Condensates with a Large Number of Vortices, Phys. Rev. Lett. **88**, 180403 (2002).

[34] S. I. Matveenko and G. V. Shlyapnikov, Tkachenko modes and their damping in the vortex lattice regime of rapidly rotating bosons, Phys. Rev. A **83**, 033604 (2011).

[35] N. R. Cooper, Rapidly rotating atomic gases, Adv. Phys. **57**, 539 (2008).

[36] M. A. Caracanhas, V. S. Bagnato, and R. G. Pereira, Tkachenko Polarons in Vortex Lattices, Phys. Rev. Lett. **111**, 115304 (2013).

[37] A. L. Fetter, Rotating trapped Bose-Einstein condensates, Rev. Mod. Phys. **81**, 647 (2009).

[38] V. Schweikhard, I. Coddington, P. Engels, V. P. Mogendorff, and E. A. Cornell, Rapidly Rotating Bose-Einstein Condensates in and near the Lowest Landau Level, Phys. Rev. Lett. **92**, 040404 (2004).

[39] I. G. Lang and Yu. A. Firsov, Kinetic Theory of semiconductors with low mobility, Zh. Eksp. Teor. Fiz. **43**, 1843 (1962) [J. Exp. Theor. Phys. **16**, 1301 (1963)].

[40] K. Agarwal, I. Martin, M. D. Lukin, and E. Demler, Polaronic model of two-level systems in amorphous solids, Phys. Rev. B **87**, 144201 (2013).

[41] D. Benjamin and E. Demler, Variational polaron method for Bose-Bose mixtures, Phys. Rev. A **89**, 033615 (2014).

[42] D. S. Rokhsar and B. G. Kotliar, Gutzwiller projection for bosons, Phys. Rev. B **44**, 10328 (1991).

[43] W. Krauth, M. Caffarel, and J.-P. Bouchaud, Gutzwiller wave function for a model of strongly interacting bosons, Phys. Rev. B **45**, 3137 (1992).

[44] M. P. Vecchi S. Kirkpatrick, and C. D. Gelatt, Optimization by simulated annealing, Science **220**, 671 (1983).

[45] T. Comparin, tcompa/BoseHubbardGutzwiller, available at https://doi.org/10.5281/zenodo.846904.

[46] K. Sheshadri, H. R. Krishnamurthy, R. Pandit, and T. V. Ramakrishnan, Superfluid and insulating phases in an interacting-Boson Model: Mean-Field Theory and the RPA, Europhys. Lett. **22**, 257 (1993).

[47] O. Dutta, M. Gajda, P. Hauke, M. Lewenstein, D.-S. Lümann, B. A. Malomed, T. Sowiński, and J. Zakrzewski, Non-standard Hubbard models in optical lattices: A review, Rep. Prog. Phys. **78**, 066001 (2015).

[48] G. D. Mahan, (ed.), *Many-Particle Physics*, 3rd ed. (Plenum, New York, 2000).

[49] C. J. Pethick and H. Smith, *Bose-Einstein Condensation in Dilute Gases*, 2nd ed. (Cambridge University Press, Cambridge, 2008).

[50] C. Menotti, C. Trefzger, and M. Lewenstein, Metastable States of a Gas of Dipolar Bosons in a 2D Optical Lattice, Phys. Rev. Lett. **98**, 235301 (2007).